Research Square

Preprints are preliminary reports that have not undergone peer review.
They should not be considered conclusive, used to inform clinical practice,
or referenced by the media as validated information.

A quantitative method to compare regional tumor contrast between prone and supine breast MRI

Brook K. Byrd
Dartmouth College
Venkataramanan Krishnaswamy
CairnSurgical, Inc
Misty J. Fox
Dartmouth-Hitchcock Medical Center
Jiang Gui
Dartmouth Geisel School of Medicine
Roberta DiFlorio
Dartmouth-Hitchcock Medical Center
Keith Paulsen
Dartmouth College
Richard J. Barth
CairnSurgical, Inc
Timothy B. Rooney (cwm4jw@hscmail.mcc.virginia.edu)
University of Virginia Health

Research Article

Keywords: Breast neoplasm, supine breast MRI, BCS planning, multimodal MRI

Posted Date: February 5th, 2024

DOI: https://doi.org/10.21203/rs.3.rs-3919303/v1

License: This work is licensed under a Creative Commons Attribution 4.0 International License. Read Full License

Additional Declarations: Competing interest reported. Venkat Krishnaswamy reports a relationship with CairnSurgical, Inc. that includes equity or stocks. Keith D. Paulsen reports a relationship with CairnSurgical, Inc. that includes consulting or advisory and equity or stocks. Richard J. Barth Jr. reports a relationship with CairnSurgical, Inc. that includes: equity or stocks. Brook Byrd reports a relationship with CairnSurgical Inc. that includes consulting or advisory. Misty Fox reports a relationship with CairnSurgical Inc. that includes consulting or advisory. Richard J. Barth Jr., Venkat Krishnaswamy, and Keith D. Paulsen have patent #US10973589B2 issued to Dartmouth College. Jiang Gui, Roberta DiFlorio and Timothy Rooney have no conflicts of interest to declare.

Abstract

Purpose

For surgical guidance applications, supine breast MRI tumor contrast should be non-inferior to prone MRI, currently considered the standard-of-care. However, comparing image contrast quantitatively between different MRI sequences and breast orientations presents a significant challenge. Herein, we present a method for quantitatively comparing regional tumor contrast in the prone and supine breast MRI orientations for the purpose of tumor localization, and we apply this framework to assess the performance of two investigational supine scans (i.e. independent and prone-to-supine, P2S) compared to diagnostic prone MRI.

Methods

Patient tumors from two studies (NCT03573804, NCT03573661) were outlined slice-by-slice by a breast radiologist using Gd-enhanced, T1-weighted MRI. Image data were derived from subjects undergoing standard-of-care prone imaging (n = 78), independent supine imaging (n = 17), and P2S supine imaging (n = 61). Normalized tumor contrast was computed between the segmented tumor and neighboring normal tissue regions and compared for statistical differences amongst cohorts and non-inferiority to prone MRI.

Results

The independent supine cohort possessed non-inferior tumor-to-fibroglandular contrast compared to prone ($p = 0.002$), while tumor-to-fibroglandular contrast from the P2S supine cohort was found inferior to the prone cohort. However, both investigational supine scans produced non-inferior tumor-to-adipose contrast when compared to prone MRI ($p < 0.001$ in both cases).

Conclusions

Regional contrast between tumor and surrounding fibroglandular tissue suffered at later timepoints observed in the P2S supine study, resulting in inferior tumor contrast. However, when contrast-enhanced supine breast MRI is acquired independently, ratiometric comparisons indicate that tumor contrast is non-inferior to prone MRI.

1. Introduction

The most sensitive imaging examination for breast cancer diagnosis remains bilateral contrast-enhanced prone breast MRI [1–4]. Standard-of-care (SoC) contrast enhanced prone MRI allows three-dimensional visualization of breast tissue in a pendent position and detects invasive cancer and enhancing ductal carcinoma in situ (DCIS) with excellent sensitivity [5–7]. Despite these advantages, prone MR images have been shown to be less effective in the context of guiding breast conserving surgery (BCS) in the supine position [8, 9], understandably due to the significant deformation of the breast tissue that occurs between the imaged prone and surgical supine positions, which changes the orientation and the position of the tumor significantly [10–12].

As one approach to address this deformation challenge, efforts to model breast tissue deformation from prone-to-supine positions have been underway [13–15]. However, these methods are often computationally expensive and often do not produce consistent, accurate results across the broad array of breast sizes and tissue densities encountered in real world settings. As an alternative solution, supine breast MRI offers tumor localizing information in an anatomically-relevant surgical position [16–20], which has been leveraged in the development and clinical testing of several image-guidance approaches with demonstrated potential for decreasing positive margins in BCS [21, 22].

Selective tumor contrast uptake and kinetics also play a critical role in accurate tumor localization and segmentation of its 3D extents, as required for MR image-guided surgery applications [21–29]. Thus, in order to reproduce the contrast kinetics of the gold standard diagnostic prone exam, supine breast MR images are generally acquired independently[17–20] in a separate imaging session, thus requiring two MRI appointments on different days. In an effort to reduce expense, time, and scheduling constraints inherent in two separate (prone and supine) imaging sessions, we developed and clinically tested a protocol to acquire supplemental supine MRIs directly after SoC diagnostic prone MRIs (i.e. prone-to-supine, P2S, imaging) within a single imaging appointment, utilizing a single contrast injection (The Prone to Supine Breast MRI Trial, #NCT03573804).

While performing a supplemental supine breast MRI immediately after a diagnostic prone breast MRI in one imaging session provides clear logistical benefits, the resulting image contrast observed in supplemental supine scans using the P2S technique has yet to be quantified or compared to SoC prone MRI or independent supine MRI [10, 12]. Such comparisons, though critical for evaluating the feasibility of the P2S technique for image-guided surgery applications, are often not straightforward as absolute contrast-enhanced MRI images are not globally comparable, due to variations in MR imaging equipment, patient-specific scan settings, choice of imaging coils used etc. As such, metrics for quantitative comparisons between diagnostic prone and supine MR image quality have not been adequately explored in prior studies [19].

To address this issue, we developed and applied a method for quantifying ratiometric image contrast associated with tumor localization (relative to adjacent background parenchymal enhancement) across multiple breast MRI exams including two investigational supine imaging protocols and a SoC prone imaging study. We then used this approach to evaluate the inferiority/non-inferiority of supine MRI tumor contrast under these two clinical exam settings relative to SoC prone MRI: 1) independent supine MRI obtained with contrast injection during an independent imaging session and 2) P2S supine obtained directly after the prone MRI with delayed contrast from the prone exam injection.

2. Methods

Image data were acquired from consenting subjects entered on one of two prospective experimental studies of technologies used for supine MRI-guided breast conserving surgery (#NCT03573804; #NCT03573661) which were approved by Dartmouth's Committee for the Protection of Human Subjects. De-identified MRI image data were provided to CairnSurgical, Inc. under a data sharing agreement.

2.1 Breast MRI Technique

Breast MRI data were acquired on either a 1.5T Siemens scanner (MAGNETOM Aera or MAGNETOM Symphony; Siemens Medical Solutions, Malvern, PA, USA), a 3.0T Siemens scanner (MAGNETOM Prisma or MAGNETOM Skyra; Siemens Medical Solutions, Malvern, PA, USA), or a 1.5T GE MRI scanner (SIGNA™ Explorer; General Electric Company, Philadelphia, PA, USA).

For prone MRI, SoC prone MRI imaging techniques and sequences were performed using either an ultrafast 3D gradient echo (GE) sequence (VIBRANT FS) on 1.5T GE scanners, or a spoiled GE sequence (3D FLASH) with spectral (Quick-FatSat) fat suppression on 1.5T and 3.0T Siemens scanners.

For supine MRI, as previously described elsewhere [27], patients are positioned supine on the scanner with their ipsilateral arm kept parallel to their body. Foam pads are placed on the patient's chest in order to support the flex body coil and minimize breast compression so that it remains in its native position as expected in surgery.

For supine image acquisition, axial T1 fat-saturated scans were acquired using either a fast-spoiled gradient echo sequence (3D LAVA-Flex) on GE 1.5T scanners, or a spoiled gradient echo sequence (3D FLASH) in combination with either spectral (Quick-FatSat) or inversion-recovery (SPAIR) fat suppression techniques on Siemens 1.5T and 3.0T scanners. Breath holds were not utilized because early feasibility studies found such efforts to be counterproductive and not reproducible across all machines and patients. Instead, the chosen supine MRI sequences relied on rapid acquisition and signal averaging techniques. Additional scanning specifications for the supine MRI sequences utilized as part of this study are provided in Table 1 for both GE and Siemens scanners.

Table 1
Supine breast MRI scan parameters

System	Sequence name	TR	TE	FOV	Matrix	Phase Direction	Flip Angle	NEX	Slice thickness	Coils
GE 1.5T	3D LAVA-Flex	6.5 ms	3.1 ms	220–280 mm	200x200	A-P	10	3	2 mm	GEM Flex Coil 16-L Array
Siemens 1.5T	3D FLASH	6.4 ms	2.6 ms	220–280 mm	384x90	R-L	10	1	2 mm	18-channel body array + spine coil (Body 18)
Siemens 3.0T	3D FLASH	4.2 ms	2.0 ms	220–280 mm	320x80	R-L	10	2	2 mm	18-channel body spine array coil (Body 18)

For contrast imaging, intravenous Gd-agent Dotarem® (gadoterate meglumine) was administered at the prescribed dose of 0.2 mL/kg. In control group MRI data, pre-Gd images were obtained prior to contrast administration, and post-Gd images were obtained 45s post Gd-administration. In the P2S protocol, post-Gd supine images were acquired on average 23.0 ± 2.7 min. after prone MRI contrast administration. Image analysis was performed on the first acquired post-Gd T1-weighted, fat-saturated scans; however, the prone and supine MRI sequence parameters varied significantly demonstrating the need for exam-independent image comparison methods.

2.2 Study Cohorts

- Prone cohort: This MRI dataset (n = 78) resulted from patients enrolled in two studies: 61 subjects participating in a Prone to Supine Breast MRI trial (#NCT03573804) and 17 individuals entered in a Pilot Multi-Institutional study (#NCT03573661). All patients demonstrated at least 1 cm of disease as measured on mammography and/or ultrasound with a histologic diagnosis of either invasive breast cancer or ductal carcinoma in situ (DCIS). The prone cohort received SoC prone MRI either immediately prior to P2S supine imaging (n = 61) or on a separate day prior to the supine MRI exam (n = 17).
- Independent supine cohort: This MRI dataset (n = 17) resulted from patients enrolled in a Pilot Multi-Institutional study (#NCT03573661) who had > 1 cm mass and received SoC prone and supine MRI on separate days/imaging sessions.
- P2S supine cohort: This MRI dataset (n = 61) resulted from patients enrolled in a Prone to Supine Breast MRI trial (#NCT03573804) who had > 1cm mass and received SoC prone MRI immediately prior to a supine MRI exam. The P2S imaging protocol involved acquisition of SoC contrast-enhanced prone MRI followed by turning the patient over to the supine position to acquire additional supine images (P2S supine) during the same imaging session and without additional contrast injection. Average time from contrast administration (prone) to start and end of the dynamic supine sequence was 23.0 ± 2.7 min. and 29.3 ± 2.9 min., respectively. SoC prone MRI data from these subjects are included in the prone cohort.

2.3 Segmentation Methods

A breast radiologist with 21 years of experience outlined tumor edges on contiguous axial MRI slices acquired with subjects positioned in prone and supine positions as illustrated in Fig. 1a. Both mass and non-mass enhancing (NME) regions were included in the radiologists' segmentation. In cases of multiple disparate lesions, only the primary lesion was segmented. A 3D tumor model was constructed using 3D Slicer (Version 4.11, www.slicer.org) on the radiologist-segmented MRI obtained from Ambra (Ambra Health Inc., New York, NY). Additional image analysis was performed in MATLAB (v.2021a).

To define tumor boundary regions, adipose and fibroglandular tissue directly surrounding the segmented tumor were selected with a margin thickness that ensured equivalent volumetric comparisons between tumor and boundary regions (Fig. 1b). Normalized tumor-to-boundary contrast was calculated as:

$$Normalized\ Contrast = \frac{I_{Tumor} - I_{Boundary}}{I_{Tumor} + I_{Boundary}} \quad (1)$$

where I_{Tumor} and $I_{Boundary}$ and represent mean tumor and boundary region intensities in MRI signal units, respectively. Dividing MR intensity differences by their sum $\left(I_{Tumor}+I_{Boundary}\right)$ ensured contrast values ranged from [-1, 1] and bounded the measurements within a constant window for global comparisons [30, 31].

Boundary regions were classified as adipose or fibroglandular using Otsu's method for intensity thresholding[32] (See Fig. 2(a-b)). In some cases, fibroglandular segmentations included pectoral muscle located within the boundary region. Resulting segmentations appear in Fig. 2(c-d). All segmentations were confirmed by the lead breast radiologist's visual inspection. Using segmented fibroglandular and adipose regions, normalized tumor-to-fibroglandular contrast was calculated according to Eq. 1 (mean tumor intensity minus mean fibroglandular intensity divided by their sum), and similarly, tumor-to-adipose contrast.

Normalized tumor-to-fibroglandular and tumor-to-adipose contrast values were compared between the prone, independent supine, and P2S supine MRI datasets. To estimate the amount of fibroglandular tissue surrounding each segmented tumor volume, a compositional percentage was calculated as volume of fibroglandular tissue in the boundary region divided by the total boundary volume.

2.4 Statistical Analysis

A series of two-sample t-tests was performed amongst the three MRI datasets (prone, independent supine, and P2S supine) for tumor-to-fibroglandular and tumor-to-adipose contrast measurements with $\alpha = 0.05$ and assumed unequal variances. To address sample size limitations, a post-hoc power (PHP) analysis was applied to generate 95% confidence intervals (CIs) and Power for each statistical test. All sample populations were confirmed to be normally distributed using the One-sample Kolmogorov-Smirnov test.

Differences between the two investigational supine scans (independent supine and P2S supine) when compared to prone were calculated with 95% CI. Non-inferiority tests were conducted on independent supine and P2S supine in which the non-inferiority margin was set to a difference of -0.1, representing a 10% decrease in normalized contrast. Using a two-sample, one-tailed t-test ($\alpha = 0.025$), the null hypothesis of inferiority was rejected if $p < 0.025$ and the 95% CI extended below the non-inferiority margin.

Tumor-to-boundary contrast was not statistically compared across cohorts because it is not a reliable measure due to varying compositions of adipose and fibroglandular tissue in the boundary regions across patients. To examine the dependence of tumor-to-boundary contrast on boundary tissue composition, we looked at the correlation between tumor-to-boundary contrast and fibroglandular boundary composition (%) in paired prone and P2S supine MRI datasets ($p = 61$) through Pearson's correlation coefficient (r) and its 95% CI.

3. Results

Distributions of tumor-to-fibroglandular and tumor-to-adipose contrast for prone, independent supine, and P2S supine datasets are shown in Fig. 3. P2S supine image data exhibited lower tumor-to-fibroglandular contrast compared to others (Fig. 3a). Using a two-sample, two-tailed t-test, mean P2S supine tumor-to-fibroglandular contrast was different statistically from the prone ($\mu_{diff} = -0.09$, 95% CI = [-0.12, -0.05], $p < 0.001$, PHP > 0.99) and independent supine cohort ($\mu_{diff} = -0.09$, 95% CI = [-0.16, -0.03], $p = 0.008$, PHP = 0.80). No statistical differences were found amongst tumor-to-adipose contrast comparisons amongst the three datasets (Fig. 3b).

Using one-sided, two-sample t-tests to test for non-inferiority (α = 0.025) and associated power calculations for 95% CI, the p-value and post-hoc power (PHP) calculations for non-inferiority of independent supine and P2S supine contrast values relative to prone measurements are displayed in Fig. 4 as forest plots with the 95% CIs for sample differences represented as solid black lines in the figure.

The non-inferiority margin [-0.10, 0] is depicted as the gray region in the plots of Fig. 4. Across both contrast metrics, the independent supine contrast was found to be statistically non-inferior to prone contrast within a margin of 0.1 normalized contrast units. For tumor-to-fibroglandular contrast (Fig. 4a), the P2S supine contrast was found to be inferior to prone, crossing over the non-inferiority margin. The P2S supine contrast values fell above the non-inferiority margin for tumor-to-adipose contrast ($p < 0.001$, PHP > 0.99); thus, we reject the null hypothesis of inferiority in this case.

As another interesting finding, negative correlations were observed between fibroglandular boundary composition (%) and resulting tumor-to-boundary contrast (Fig. 5). The linear relationships for the paired prone (Pearson's r = -0.50, [-0.67, -0.29]) and P2S supine (Pearson's r = -0.57 [-0.72, -0.37]) datasets exhibited similar negative trends. Cases with high amounts of fibroglandular tissue in the tumor boundary often resulted in reduced tumor-to-boundary contrast as demonstrated in Fig. 5 (c-d) with 84% and 79% fibroglandular boundary composition, respectively.

4. Discussion

While previous studies have reported on supine MRI feasibility [17, 19, 20, 33], prone vs. supine MRI characteristics [11, 33, 34], and prone-to-supine (P2S) MRI study results [10, 12], tumor contrast has yet to be systematically compared between prone and supine breast MRI scans. To address this gap, we utilized ratiometric contrast measurements to compare prone and supine breast MRI acquisitions and assess acceptability of investigational supine MRI (as non-inferior to prone breast MRI tumor contrast) for the first time. Our results showed no statistical difference in tumor contrast between prone and supine breast MRI when acquired separately (independent supine MRI) and suggest that breast orientation change from prone (for SoC imaging) to supine (for surgical planning) is acceptable, clinically, for determining MRI-defined tumor extent in the supine position.

While supine MRI has been demonstrated to produce images of excellent quality using clinically available MRI machines, coils, and sequences;[17, 24, 34, 35] supine MRI is not a replacement for diagnostic prone MRI. From a diagnostic perspective, the prone pendant breast position is advantageous for examining disease extension with little to no respiratory motion artifacts. On the contrary, respiratory motion during ungated supine MRI scans can cause streaking artifacts in the phase encode direction, directly resulting in displaced tissue signal and degraded image quality.[17]

Although motivation to perform prone-to-supine MRI within a single imaging session is strong, the sufficiency of tumor contrast in supplemental supine scans for margin delineation has not been quantified previously. Amongst the two published P2S studies [10, 12], both reported on observed lesion displacement from prone-to-supine patient positioning, but did not otherwise examine tumor contrast. Aribal et al. (2019) did investigate the radiologists' ability to detect lesions in supine MRI [12]. However, detecting tumor vs. determining its extent are different tasks, the latter requiring high fidelity in tumor margin delineation, which can be evaluated quantitatively

by assessing tumor contrast. Our approach was designed to assess image contrast as it relates to segmenting tumor extent in a 3D volume – an important step in surgical planning for optimal (margin negative) breast conserving surgery [22].

P2S supine MRI (without additional contrast injection after the prone MRI) demonstrated inferior tumor contrast relative to SoC prone tumor contrast, with lower tumor-to-fibroglandular contrast found in the P2S supine MRI data. Loss of contrast at later time points (average delay time = 23 min.) may be explained by known Gd-kinetics in which fibroglandular tissue often shows persistent Gd-uptake while tumorous regions washout the Gd-based contrast in the later phases of image acquisition [36, 37].

Unlike the P2S supine image data, independent supine (separate imaging session) MRI exhibited non-inferior contrast compared to prone, indicating that independent supine imaging can produce non-inferior tumor-to-fibroglandular contrast when compared to SoC prone MRI. While supine MRI achieves tumor contrast comparable to prone MRI when acquired separately, patient and clinical care demands associated with multiple visits suggest a single imaging session solution is needed. Given these preliminary prone-to-supine results, a secondary prone-to-supine study is underway which utilizes two boluses, one before prone and one before supine acquisitions, in a single imaging exam session (ClinicalTrials.gov, # NCT00159939). Moving forward, the ratiometric contrast approach used here is a powerful tool for examining and comparing image contrast amongst multiple MRI sequences and breast exam protocols independent of patient orientation or image sequence.

By partitioning regional tumor contrast into tumor-to-fibroglandular and tumor-to-adipose categories, differences associated with specific types of surrounding tissue were identified; however, patient-specific factors such as disease type, lesion type, and receptor status were not examined. In addition, the cohort sizes of each imaging procedure compared were different (independent supine n = 17, P2S supine n = 61, and prone n = 78) due to the differing sizes of two clinical trials. Additional statistical measures were taken to ensure a fair comparison amongst cohorts including Kolmogorov-Smirnov tests for sample normalcy, post-hoc power analysis, and assumptions of non-equal variance amongst the three cohorts.

5. Conclusions

The ratiometric contrast method presented herein enabled quantitative comparisons of regional tumor contrast amongst standard-of-care prone and investigational supine breast MRI datasets. When acquired separately, supine MRI produced non-inferior tumor contrast compared to prone MRI. Confirming non-inferiority of supine breast MRI contrast for the first time increases confidence that the breast orientation change from prone (for SoC imaging) to supine (for surgical planning) will have a positive clinical impact on BCS outcomes. However, regional contrast between tumor and surrounding fibroglandular tissue suffered in later timepoints observed in the P2S supine study, resulting in inferior P2S supine image contrast suggesting that further work is needed to acquire prone and supine image data with non-inferior tumor contrast within a single breast MRI exam session.

Declarations

Author Contribution

T.R. and B.B. contributed to the original draft and formal analysis, while V.K. and T.R. handled visualization. B.B. led software development and data curation. V.K. supervised the project, managed administration, secured funding, and played a role in conceptualization. M.F. and J.G. contributed to methodology and investigation, with R.D. assisting in investigation. K.P. and R.B. were involved in conceptualization, methodology, and manuscript work. T.R. participated in all phases, including supervision, original draft preparation, and manuscript review.

Acknowledgements

This work was supported by the National Institutes of Health/National Cancer Institute (NIH/NCI) Small Business Innovation Research grants R44CA210810 and R44CA232862 to CairnSurgical, Inc (PI: Krishnaswamy).

Disclosure Statement

Venkat Krishnaswamy reports a relationship with CairnSurgical, Inc. that includes equity or stocks. Keith D. Paulsen reports a relationship with CairnSurgical, Inc. that includes consulting or advisory and equity or stocks. Richard J. Barth Jr. reports a relationship with CairnSurgical, Inc. that includes: equity or stocks. Brook Byrd reports a relationship with CairnSurgical Inc. that includes consulting or advisory. Misty Fox reports a relationship with CairnSurgical Inc. that includes consulting or advisory. Richard J. Barth Jr., Venkat Krishnaswamy, and Keith D. Paulsen have patent #US10973589B2 issued to Dartmouth College. Jiang Gui, Roberta DiFlorio and Timothy Rooney have no conflicts of interest to declare.

Data Availability Statement

The datasets generated during and/or analyzed during the current study are available from the corresponding author on reasonable request.

References

1. Sardanelli F, Giuseppetti GM, Panizza P, et al (2004) Sensitivity of MRI Versus Mammography for Detecting Foci of Multifocal, Multicentric Breast Cancer in Fatty and Dense Breasts Using the Whole-Breast Pathologic Examination as a Gold Standard. American Journal of Roentgenology 183:1149–1157. https://doi.org/10.2214/ajr.183.4.1831149
2. Schnall MD, Blume J, Bluemke DA, et al (2005) MRI detection of distinct incidental cancer in women with primary breast cancer studied in IBMC 6883. J Surg Oncol 92:32–38. https://doi.org/10.1002/jso.20381
3. Lehman CD, DeMartini W, Anderson BO, Edge SB (2009) Indications for Breast MRI in the Patient with Newly Diagnosed Breast Cancer. J Natl Compr Canc Netw 7:193–201. https://doi.org/10.6004/jnccn.2009.0013
4. Newman LA (2020) Role of Preoperative MRI in the Management of Newly Diagnosed Breast Cancer Patients. Journal of the American College of Surgeons 230:331–339. https://doi.org/10.1016/j.jamcollsurg.2019.12.004
5. Kim DY, Moon WK, Cho N, et al (2007) MRI of the Breast for the Detection and Assessment of the Size of Ductal Carcinoma in Situ. Korean J Radiol 8:32. https://doi.org/10.3348/kjr.2007.8.1.32
6. Lehman CD (2010) Magnetic Resonance Imaging in the Evaluation of Ductal Carcinoma In Situ. JNCI Monographs 2010:150–151. https://doi.org/10.1093/jncimonographs/lgq030

7. Baur A, Bahrs SD, Speck S, et al (2013) Breast MRI of pure ductal carcinoma in situ: Sensitivity of diagnosis and influence of lesion characteristics. European Journal of Radiology 82:1731–1737. https://doi.org/10.1016/j.ejrad.2013.05.002
8. Turnbull L, Brown S, Harvey I, et al (2010) Comparative effectiveness of MRI in breast cancer (COMICE) trial: a randomised controlled trial. The Lancet 375:563–571. https://doi.org/10.1016/S0140-6736(09)62070-5
9. Peters NHGM, van Esser S, van den Bosch MAAJ, et al (2011) Preoperative MRI and surgical management in patients with nonpalpable breast cancer: The MONET – Randomised controlled trial. European Journal of Cancer 47:879–886. https://doi.org/10.1016/j.ejca.2010.11.035
10. Carbonaro LA, Tannaphai P, Trimboli RM, et al (2012) Contrast enhanced breast MRI: Spatial displacement from prone to supine patient's position. Preliminary results. European Journal of Radiology 81:e771–e774. https://doi.org/10.1016/j.ejrad.2012.02.013
11. Gombos EC, Jayender J, Richman DM, et al (2016) Intraoperative Supine Breast MR Imaging to Quantify Tumor Deformation and Detection of Residual Breast Cancer: Preliminary Results. Radiology 281:720–729. https://doi.org/10.1148/radiol.2016151472
12. Aribal E, Bugdayci O (2019) Supplementary abbreviated supine breast MRI following a standard prone breast MRI with single contrast administration: is it effective in detecting the initial contrast-enhancing lesions? Diagn Interv Radiol 25:265–269. https://doi.org/10.5152/dir.2019.18167
13. Rajagopal V, Lee A, Chung J-H, et al (2008) Creating Individual-specific Biomechanical Models of the Breast for Medical Image Analysis. Academic Radiology 15:1425–1436. https://doi.org/10.1016/j.acra.2008.07.017
14. Lianghao Han, Hipwell JH, Eiben B, et al (2014) A Nonlinear Biomechanical Model Based Registration Method for Aligning Prone and Supine MR Breast Images. IEEE Trans Med Imaging 33:682–694. https://doi.org/10.1109/TMI.2013.2294539
15. Eiben B, Vavourakis V, Hipwell JH, et al (2016) Symmetric Biomechanically Guided Prone-to-Supine Breast Image Registration. Ann Biomed Eng 44:154–173. https://doi.org/10.1007/s10439-015-1496-z
16. Alderliesten T, Loo C, Paape A, et al (2010) On the feasibility of MRI-guided navigation to demarcate breast cancer for breast-conserving surgery: MRI-guided breast cancer demarcation. Med Phys 37:2617–2626. https://doi.org/10.1118/1.3429048
17. Siegler P, Holloway CMB, Causer P, et al (2011) Supine breast MRI. J Magn Reson Imaging 34:1212–1217. https://doi.org/10.1002/jmri.22605
18. Joukainen S, Masarwah A, Könönen M, et al (2019) Feasibility of mapping breast cancer with supine breast MRI in patients scheduled for oncoplastic surgery. Eur Radiol 29:1435–1443. https://doi.org/10.1007/s00330-018-5681-y
19. Fausto A, Fanizzi A, Volterrani L, et al (2020) Feasibility, Image Quality and Clinical Evaluation of Contrast-Enhanced Breast MRI Performed in a Supine Position Compared to the Standard Prone Position. Cancers 12:2364. https://doi.org/10.3390/cancers12092364
20. Siegler P, Ebrahimi M, Holloway CMB, et al (2012) Supine breast MRI and assessment of future clinical applications. European Journal of Radiology 81:S153–S155. https://doi.org/10.1016/S0720-048X(12)70064-5
21. Sakakibara M, Nagashima T, Sangai T, et al (2008) Breast-Conserving Surgery Using Projection and Reproduction Techniques of Surgical-Position Breast MRI in Patients with Ductal Carcinoma In Situ of the

Breast. Journal of the American College of Surgeons 207:62–68. https://doi.org/10.1016/j.jamcollsurg.2007.12.034

22. Barth RJ, Krishnaswamy V, Paulsen KD, et al (2019) A Randomized Prospective Trial of Supine MRI-Guided Versus Wire-Localized Lumpectomy for Breast Cancer. Ann Surg Oncol 26:3099–3108. https://doi.org/10.1245/s10434-019-07531-4
23. Pallone MJ, Poplack SP, Avutu HBR, et al (2014) Supine Breast MRI and 3D Optical Scanning: A Novel Approach to Improve Tumor Localization for Breast Conserving Surgery. Ann Surg Oncol 21:2203–2208. https://doi.org/10.1245/s10434-014-3598-5
24. Sakakibara M, Yokomizo J, Shiina N, et al (2014) MRI-Guided Quadrantectomy in Patients with Ductal Carcinoma in Situ Detected Preoperatively by Mammographic Calcifications. Journal of the American College of Surgeons 219:295–302. https://doi.org/10.1016/j.jamcollsurg.2014.02.025
25. Barth RJ, Krishnaswamy V, Paulsen KD, et al (2017) A Patient-Specific 3D-Printed Form Accurately Transfers Supine MRI-Derived Tumor Localization Information to Guide Breast-Conserving Surgery. Ann Surg Oncol 24:2950–2956. https://doi.org/10.1245/s10434-017-5979-z
26. Perkins SL, Lin MA, Srinivasan S, et al (2017) A Mixed-Reality System for Breast Surgical Planning. In: 2017 IEEE International Symposium on Mixed and Augmented Reality (ISMAR-Adjunct). IEEE, Nantes, France, pp 269–274
27. Barth RJ, Krishnaswamy V, Rooney TB, et al (2022) A pilot multi-institutional study to evaluate the accuracy of a supine MRI based guidance system, the Breast Cancer Locator^{TM}, in patients with palpable breast cancer. Surgical Oncology 44:101843. https://doi.org/10.1016/j.suronc.2022.101843
28. Lee HS, Kim HJ, Chung IY, et al (2021) Usefulness of 3D-surgical guides in breast conserving surgery after neoadjuvant treatment. Sci Rep 11:3376. https://doi.org/10.1038/s41598-021-83114-2
29. Wu Z-Y, Kim HJ, Lee J, et al (2021) Breast-conserving surgery with 3D-printed surgical guide: a single-center, prospective clinical study. Sci Rep 11:2252. https://doi.org/10.1038/s41598-021-81936-8
30. Oak PV, Kamathe R Contrast enhancement of brain MRI images using histogram based techniques
31. Senthilkumaran N, Thimmiaraja J (2014) Histogram Equalization for Image Enhancement Using MRI Brain Images. In: 2014 World Congress on Computing and Communication Technologies. IEEE, Trichirappalli, India, pp 80–83
32. Otsu N (1979) A Threshold Selection Method from Gray-Level Histograms. IEEE Trans Syst, Man, Cybern 9:62–66. https://doi.org/10.1109/TSMC.1979.4310076
33. Joukainen S, Masarwah A, Könönen M, et al (2019) Feasibility of mapping breast cancer with supine breast MRI in patients scheduled for oncoplastic surgery. Eur Radiol 29:1435–1443. https://doi.org/10.1007/s00330-018-5681-y
34. Fausto A, Fanizzi A, Volterrani L, et al (2020) Feasibility, Image Quality and Clinical Evaluation of Contrast-Enhanced Breast MRI Performed in a Supine Position Compared to the Standard Prone Position. Cancers 12:2364. https://doi.org/10.3390/cancers12092364
35. Byrd BK, Krishnaswamy V, Gui J, et al (2020) The shape of breast cancer. Breast Cancer Res Treat 183:403–410. https://doi.org/10.1007/s10549-020-05780-6
36. Agrawal G, Su M-Y, Nalcioglu O, et al (2009) Significance of breast lesion descriptors in the ACR BI-RADS MRI lexicon. Cancer 115:1363–1380. https://doi.org/10.1002/cncr.24156

37. Cheng L, Li X (2013) Breast magnetic resonance imaging: kinetic curve assessment. Gland Surgery 2:50. https://doi.org/10.3978/j.issn.2227-684X.2013.02.04

Figures

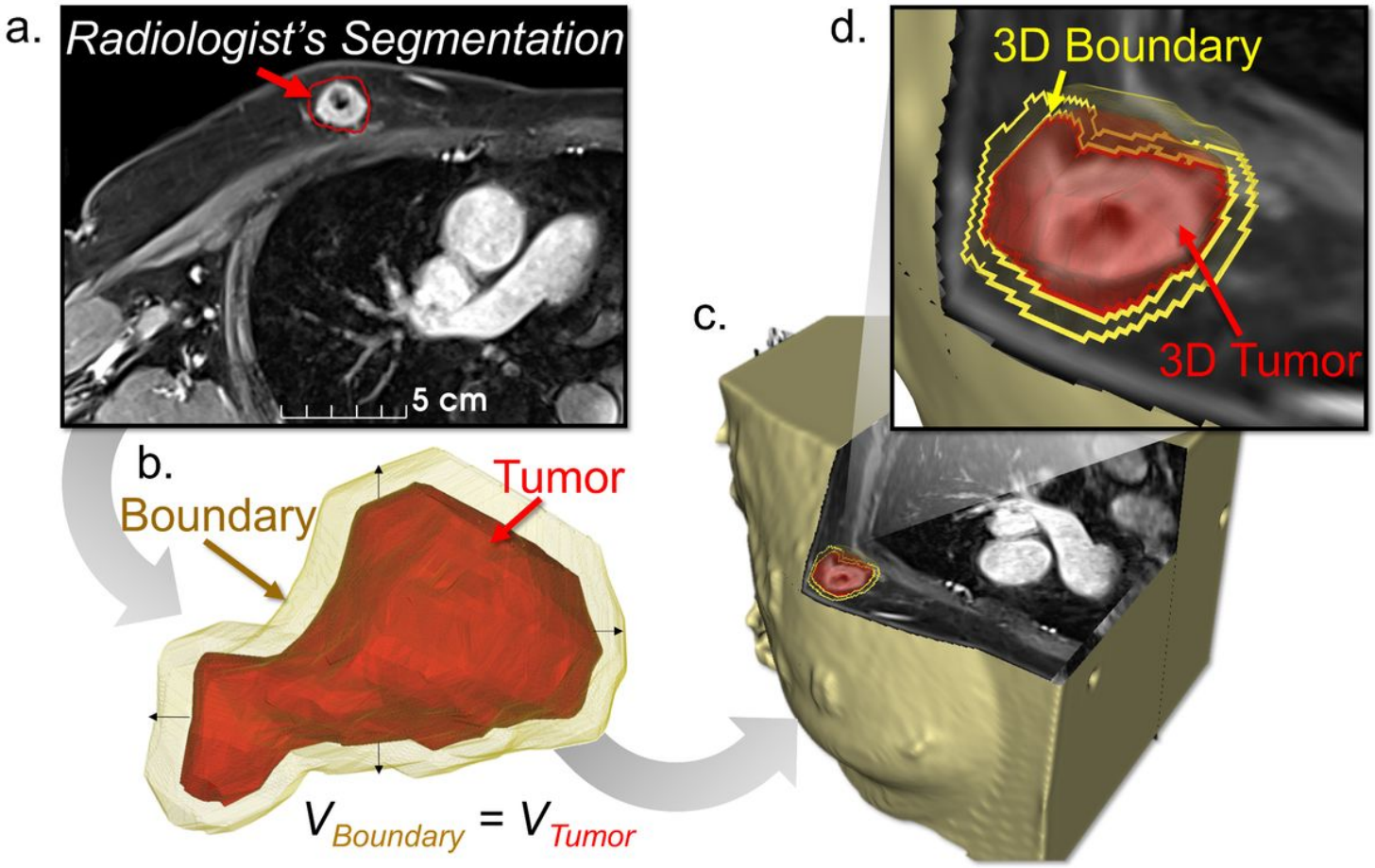


Figure 1

(a) Radiologist's slice-by-slice segmentation of tumor region, (b) 3D rendered tumor model and surrounding boundary regions, (c) Segmentations overlaid onto MRI volume with (d) tumor and boundary voxel regions identified.

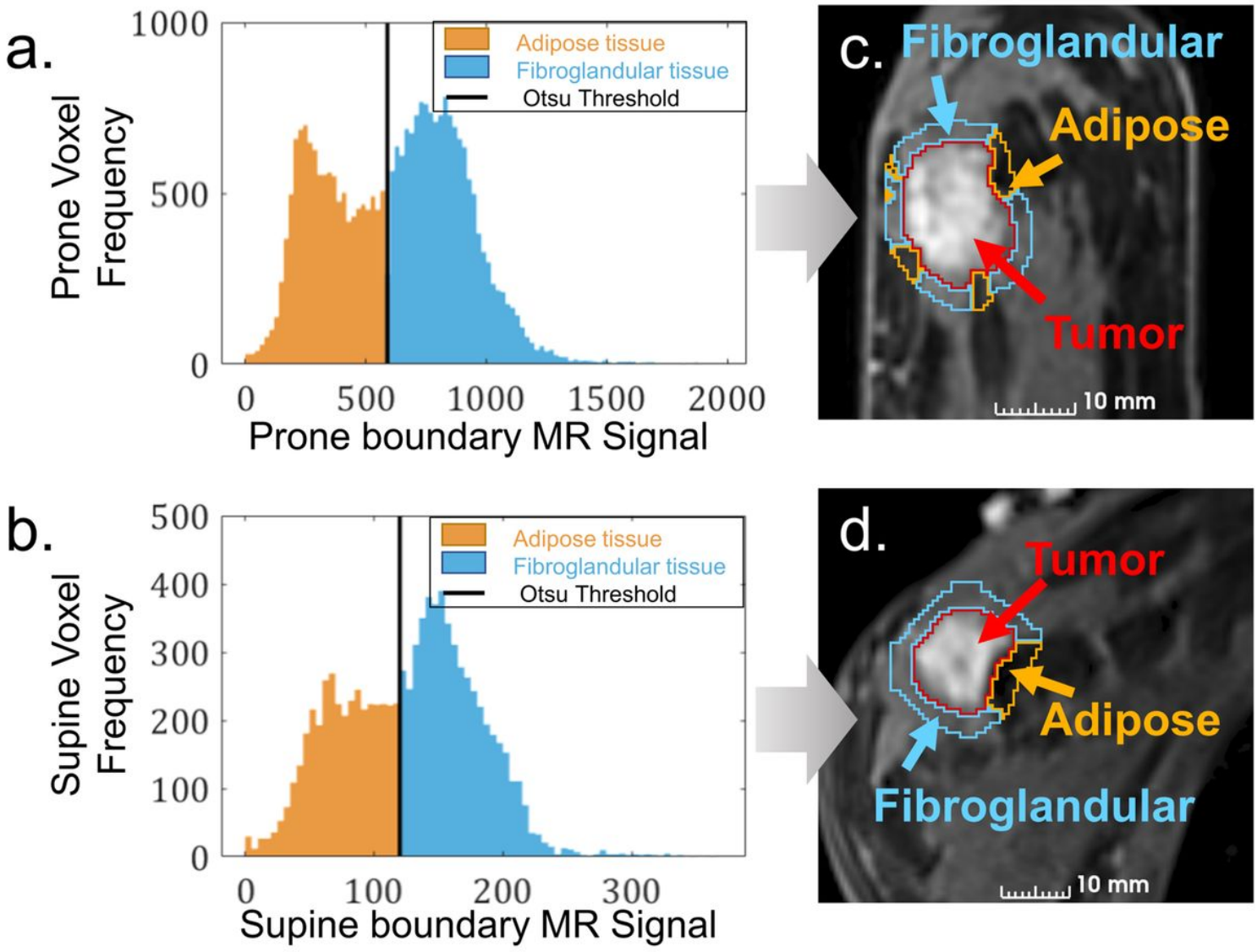


Figure 2

Exemplary boundary tissue MRI signal intensity histograms with Otsu thresholding to distinguish adipose from fibroglandular in (a) prone and (c) supine orientations. Resulting segmentations distinguish tumor-surrounding adipose (orange) from fibroglandular tissues (blue) in the (c) prone and (d) supine MRI.

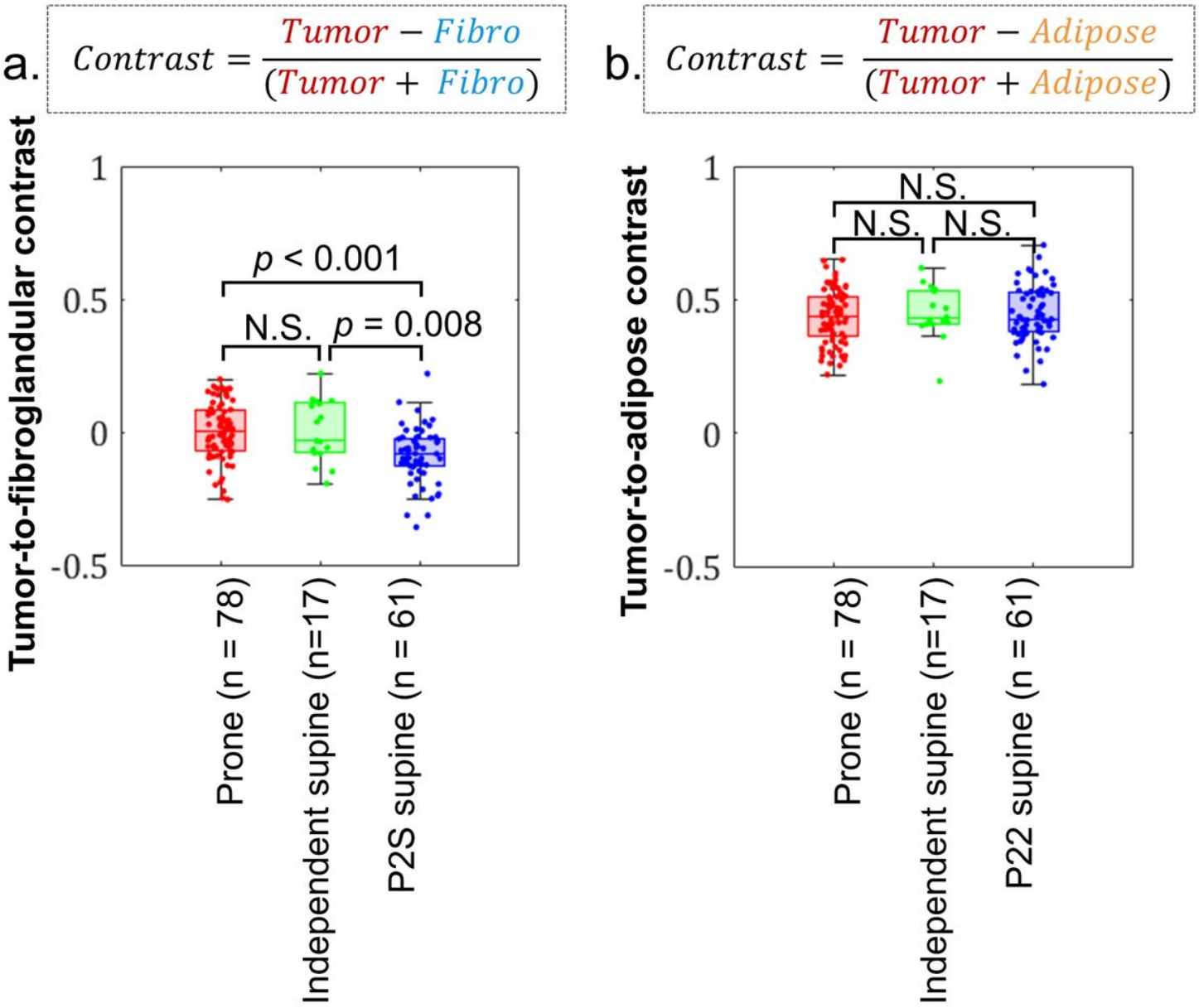


Figure 3

Boxplot distributions and two-sample, t-test statistical outcomes for comparisons between prone, independent supine, and P2S supine image data for (a) tumor-to-fibroglandular and (b) tumor-to-adipose contrasts

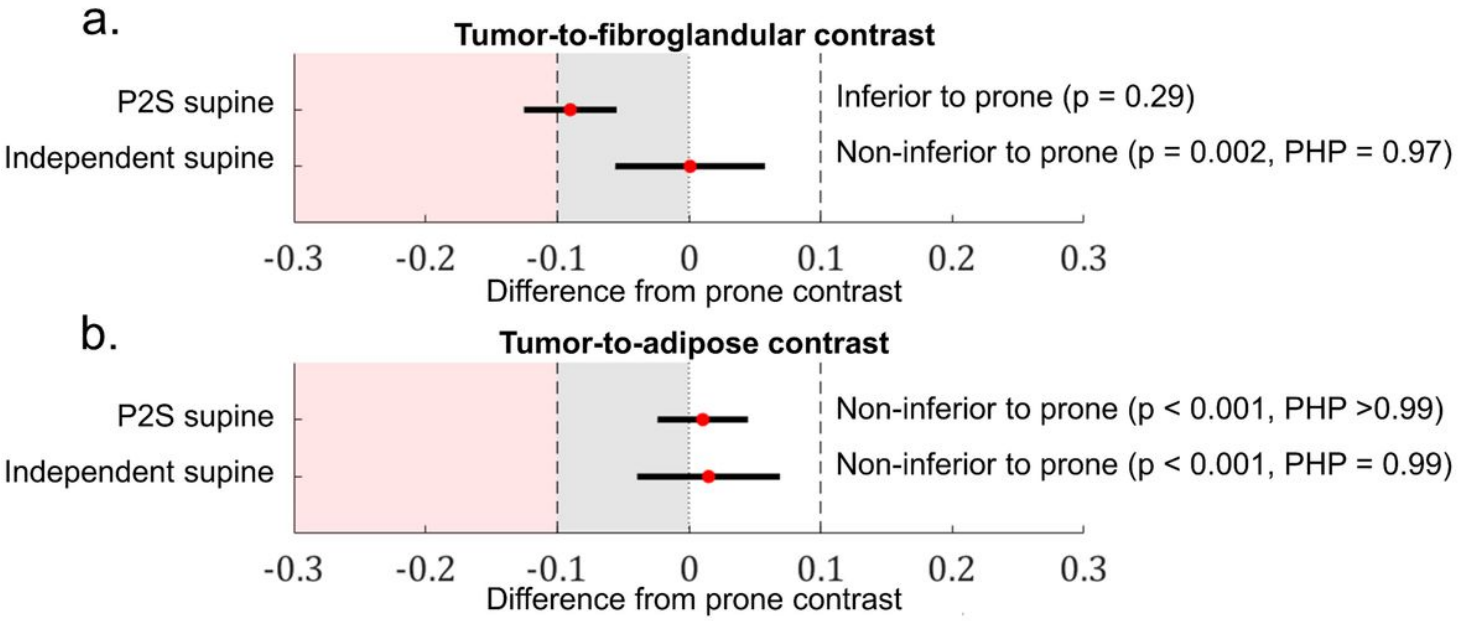


Figure 4

Forest plots exhibiting differences from the prone contrast values for P2S supine and independent supine measurements of (a) tumor-to-fibroglandular and (b) tumor-to-adipose normalized contrasts. The non-inferiority margin (grey) was set to be a difference of 0.1 from the prone contrast measurement.

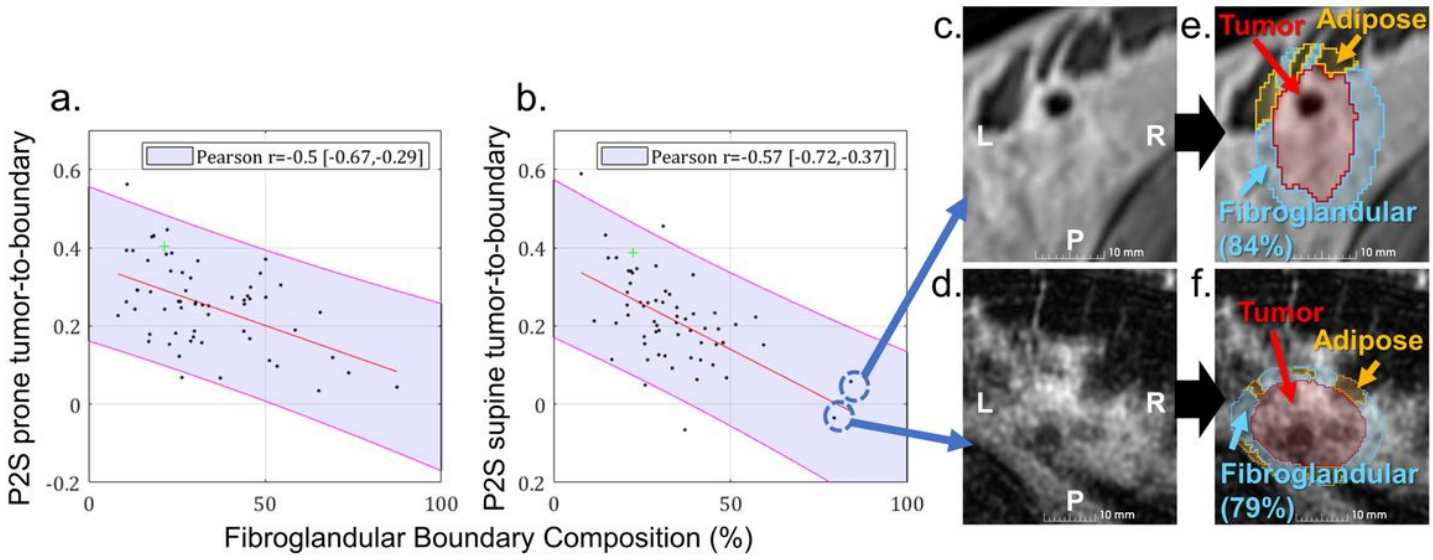


Figure 5

Correlation between tumor-to-boundary contrast and fibroglandular boundary composition (%) for the P2S cohort's (a) prone MRI and (b) P2S supine MRI datasets (n = 61). (c-d) T1-weighted MRI examples from the P2S supine dataset exhibiting high fibroglandular composition (%) around the tumor region with (e-f) overlaid labels.